# Investigation of the Platinum Cluster Size and Location on Zeolite KL with $^{129}$Xe NMR, XAFS, and Xenon Adsorption

**Sung June Cho, Wha-Seung Ahn,† Suk Bong Hong,‡ and Ryong Ryoo***

*Department of Chemistry and Center for Molecular Science, Korea Advanced Institute of Science and Technology, Taeduk Science Town, Taejon, 305-701 Korea*

*Received: September 5, 1995; In Final Form: November 30, 1995*[⊗]

Although platinum clusters supported on zeolite KL (Pt/KL) were extensively investigated by other laboratories due to remarkable catalytic activity and selectivity for the conversion of linear alkanes to aromatic compounds, there was still some controversy over the cluster size and location in the zeolite channel. The controversy came from difficulty in obtaining high Pt content suitable for the physical characterization without altering the cluster size, compared with the practical catalyst samples. In the present study, we were able to increase the Pt content to 5.2 wt % without changing the physical properties of the Pt/KL, following a procedure using the ion exchange of $Pt(NH_3)_4^{2+}$. We have characterized the Pt cluster size and location on the zeolite using the chemical shift in $^{129}$Xe NMR spectroscopy of adsorbed xenon and the X-ray absorption fine structure (XAFS) obtained at the Pt $L_{III}$ edge. Results from the $^{129}$Xe NMR and XAFS indicate that the Pt cluster consisted of five to seven Pt atoms located inside the zeolite main channel which is formed by interconnection of cages 1.1 nm in diameter to each other in a linear way through 0.71-nm apertures. The Pt cluster has been found to chemisorb approximately two hydrogen atoms per *total* Pt at 296 K. The Pt cluster adsorbed as much as 0.4 Xe/Pt at 296 K, which is much more than 0.07 Xe/Pt obtained for a 1-nm Pt cluster entrapped inside the supercage of zeolite NaY (Pt/NaY) under the same conditions. It is believed that a cluster consisting of more than five to seven Pt atoms had difficultly adsorbing such a large quantity of xenon under the experimental condition. The small Pt cluster did not cause considerable pore blockage against the adsorption of Xe (0.43 nm in diameter) and $CCl_4$ (0.59 nm in diameter) into the zeolite pore, indicating the location at a bulged part within the 1.1-nm pore.

## Introduction

Zeolite LTL is a crystalline aluminosilicate molecular sieve with a microporous channel formed by linear interconnection of lobe-shaped cages (1.1 nm in diameter, 0.6 nm in length) through apertures of 0.71 nm in diameter.[1] The Si/Al ratio for the zeolite is typically 3.0, and the zeolite is synthesized with $K^+$ ion compensating a negative charge at the $AlO_4$ unit.

Platinum clusters supported on the $K^+$-ionic form of zeolite LTL (Pt/KL) attract much attention due to very high catalytic activity and selectivity for the conversion of linear paraffins to aromatic compounds.[2] The location and size of the Pt clusters in the KL zeolite have been investigated by many laboratories trying to understand the unique catalytic property which seems to come from shape selectivity of the zeolite channel as well as the electronic effect due to small cluster size.[3−6] These works have reported on the estimation of the Pt cluster size using the Pt−Pt coordination number (CN) obtained through curve fitting of the X-ray absorption fine structure (XAFS) of Pt measured at the Pt $L_{III}$ edge. However, the Pt−Pt CN by the works shows considerable differences over the range between 3.7 and 7.1.[4−6] This CN range includes Pt clusters consisting of five to thirty atoms. A Pt cluster with five atoms in the zeolite channel should be small enough to allow the diffusion of *n*-hexane and benzene through the zeolite channel in the presence of the cluster, while a Pt cluster with the CN equal to 7.1 would be large enough to cause the pore blockage.

Studies on Pt clusters supported on zeolite NaY (Pt/NaY) have shown that the cluster size and location is sensitive to not only supporting methods (e.g., ion exchange and impregnation) but also detailed experimental conditions such as Pt wt %, heating temperatures, and heating rates for the activation and reduction treatments.[7] Such sensitivity of the cluster size to preparation conditions seems to be responsible for differences in the Pt−Pt CN for Pt/KL. Hydrogen chemisorption on Pt/KL measured volumetrically at room temperature also shows differences between 0.6 and 2.1 H/Pt.[3−6] High ratios approaching 2 H/Pt for *total* chemisorption of hydrogen per *total* platinum are obtained for samples with Pt content much lower than 1 wt %.[3c,4,5] However, prior to the present work, it was not clear if the high H/Pt ratios came from small Pt cluster sizes or hydrogen spillover to the support.

Recently, we have investigated the effect of sample preparation conditions on hydrogen chemisorption of Pt/KL.[8] We have confirmed that hydrogen chemisorption depends significantly on experimental methods and conditions used for supporting Pt clusters. The hydrogen chemisorption increased when the Pt cluster was prepared by an ion exchange method using $Pt(NH_3)_4(NO_3)_2$, compared to impregnation using $H_2PtCl_6$. When temperatures for the platinum activation and reduction were increased very slowly to 573 K after the ion exchange of $Pt(NH_3)_4(NO_3)_2$, the Pt cluster chemisorbed as much as a *total* of two H atoms per *total* Pt.

In the present work, we have obtained four Pt/KL samples containing 0.9, 2.0, 3.4, and 5.2 wt % Pt using the above ion exchange procedure, respectively. In spite of a 6-fold variation in the Pt loading, hydrogen chemisorption changed very little from 2 $H_{total}/Pt_{total}$. The samples showed high activity and selectivity for catalytic conversion of *n*-hexane to benzene, similar to those reported by others.[3,9] The turnover frequency ($\nu_t$), i.e., the number of hexane molecules converted per Pt atom during 1 s, decreased to about the 40% level as the Pt loading

* To whom all correspondence should be addressed.
† Department of Chemical Engineering, Inha University, Incheon, 402-501 Korea.
‡ Korea Institute of Science and Technology, P.O. Box 131, Cheongryang, Seoul, 130-650 Korea.
⊗ Abstract published in *Advance ACS Abstracts,* February 15, 1996.

0022-3654/96/20100-4996$12.00/0 

increased from 0.9 to 5.2 wt %. This decent change in $\upsilon_t$ compared with the Pt content may be attributed to only a diffusion limitation, and therefore the cluster size and location for the samples did not seem to be affected considerably by the Pt wt % increase. We report here on the characterization of the cluster size and location for the Pt/KL samples using the chemical shift in $^{129}$Xe NMR spectroscopy of adsorbed xenon and the Pt−Pt CN obtained from XAFS. An additional experimental technique presented for the characterization of the Pt cluster is the determination of xenon adsorption on the Pt cluster, which is obtained from a decrease in the xenon adsorption isotherm occurring for Pt/KL upon hydrogen chemisorption on the Pt cluster.[7a,10−12] This xenon adsorption method is very sensitive to the cluster size located inside zeolite cages. Adsorption isotherms of xenon (atomic diameter 0.43 nm) and $CCl_4$ (molecular size 0.59 nm) are also shown in the present paper, to estimate the size of zeolite pore opening in the presence of the Pt cluster.

## Experimental Section

**Sample Preparation.** Experimental procedures for the preparation and characterization of Pt/KL samples are the same as those used for Pt/NaY and Pt/EMT in our previous works.[10,11] A KL zeolite sample was obtained from Union Carbide (ELZ-L, mean crystal size 1.0 $\mu$m, unit cell formula $K_9[(AlO_2)_9(SiO_2)_{27}]$). The powder zeolite was added into aqueous solutions (100 mL g$^{-1}$ zeolite) containing $0.5 \times 10^{-3}$ to $3.0 \times 10^{-3}$ mol $[Pt(NH_3)_4][NO_3]_2$ (Aldrich) per liter, and the resulting mixture was slurried overnight at room temperature. Inductively coupled plasma (ICP, Shimadzu, ICPS-100III) emission spectra of the supernatant solutions showed complete ion exchange of $Pt(NH_3)_4^{2+}$ into the zeolite during this period. The ion-exchanged zeolite was filtered, washed with doubly distilled water, dried in a vacuum oven at room temperature, and subsequently placed on a fritted disk inside a Pyrex U-tube flow reactor.

The platinum species in the zeolite sample was activated by heating in $O_2$ flow dried through a molecular sieve trap. The gas flow rate was 1 L min$^{-1}$ g$^{-1}$. The heating temperature was linearly increased from room temperature to 593 K over 12 h and then maintained at 593 K for 2 h. The gas flow rate was 1 L min$^{-1}$ g$^{-1}$. After the activation treatment was over, the $O_2$ gas was evacuated from the reactor at 573 K. Subsequently, the Pt species was reduced with heating in $H_2$ flow (99.999%, passed through a $MnO/SiO_2$ trap). The $H_2$ flow rate for the reduction was 200 mL min$^{-1}$ g$^{-1}$, and the reduction temperature was linearly increased from room temperature to 573 K over 4 h and maintained at 573 K for 2 h.

The platinum reduction was followed by evacuation under a nominal pressure of $1 \times 10^{-3}$ Pa, while the temperature was linearly increased from 573 to 673 K over 1 h and maintained at 673 K for 2 h, to remove chemisorbed hydrogen. A small portion of the Pt/KL sample thus prepared was sealed in a special NMR tube for *in situ* characterization by $^{129}$Xe NMR spectroscopy. The rest of the sample was open to air at room temperature and stored in a sample vial. The air-exposed sample was reduced again with $H_2$ flow for 1 h at 573 K and subsequently evacuated for 1 h at 673 K. This sample was also sealed in a NMR tube and characterized with $^{129}$Xe NMR. The two $^{129}$Xe NMR measurements, *in situ* and reduced again after air exposure, showed no significant difference in the chemical shifts. Therefore, the two sample treatment methods were used without distinction for further characterization.

Pt content of Pt/KL samples was determined with ICP. Samples are denoted by *x* wt % Pt/KL according to the Pt content after full dehydration.

***n*-Hexane Aromatization.** The rate of catalytic reforming of *n*-hexane was measured with typically 50 mg of catalyst using a Pyrex batch recirculation rig. The reactant gas consisted of *n*-hexane, $H_2$, and He with partial pressures of 6, 36, and 59 kPa, respectively. The *n*-hexane (Merck, HPLC grade) was used after purification through three freeze−evacuation−thaw cycles. The total volume of the rig was 620 mL. The gas recirculation rate was 4.0 L min$^{-1}$. The reaction temperature was controlled to 686 ± 1 K. Products were analyzed with a gas chromatograph (HP 5890 Series II) equipped with a Carbowax 20M column using a flame ionization detector. The total number of *n*-hexane converted per Pt was defined as the turnover number ($N_t$), based on the total number of Pt atoms. The $N_t$ was plotted against reaction time. The plot showed curvatures due to progressive catalyst deactivation with reaction time. To avoid complication by deactivation, the catalytic activity of different samples was reported as average turnover frequencies ($\upsilon_t$) taken in the same $N_t$ range of 10−30.

**Volumetric Adsorption.** Adsorption isotherms for $H_2$, Xe, and $CCl_4$ on Pt/KL were measured using a volumetric gas adsorption apparatus. Natural xenon gas (Matheson, 99.995%) was used for the adsorption measurement as well as the $^{129}$Xe NMR experiment. Liquid $CCl_4$ (Junsei, >99.5%) was vaporized into a flask and purified through three freeze−evacuation−thaw cycles, before use for adsorption measurement. The adsorption temperature was controlled to 296 ± 0.1 K by a constant-temperature circulation bath.

**$^{129}$Xe NMR.** For the $^{129}$Xe NMR experiment, a special $^{129}$Xe NMR tube equipped with high-vacuum stopcocks was joined to the above U-tube reactor by glass blowing before the powder sample was placed into the reactor. After the sample was reduced and evacuated, a 0.2−1.0-g portion was transferred from the reactor to the NMR tube by tilting the reactor, and then the tube was sealed with a flame. Xenon gas was equilibrated with the sample to a desired pressure at 296 K through the vacuum stopcocks. $^{129}$Xe NMR spectra were obtained from the adsorbed gas at 296 K with a Bruker AM 300 instrument operating at 83.0 MHz for $^{129}$Xe with a 0.5-s relaxation delay. The chemical shift is referenced to xenon gas extrapolated to zero pressure.

**XAFS.** XAFS for 2.0, 3.4, and 5.2 wt % Pt/KL samples were obtained with wafers of 10 mm in diameter pressed with 0.20-, 0.15-, and 0.10-g powder samples, respectively. Since the sample wafers were exposed to air during the wafer pressing, each wafer was reduced again with $H_2$ flow at 573 K inside a Pyrex U-tube flow reactor. The sample wafer was then moved to a joining XAFS cell, similar to the $^{129}$Xe NMR experiment. The XAFS cell was fabricated with Pyrex glass and Kapton windows (DuPont, 125 $\mu$m thick). The Kapton windows were joined using Torr Seal (Varian). The XAFS cell containing sample wafer under $H_2$ gas was sealed with a flame and stored in a vacuum desiccator until the XAFS measurement. The XAFS in $H_2$ gas was measured at the Pt $L_{III}$ edge at room temperature using the Beam Line 10B at the Photon Factory in Tsukuba. The XAFS of Pt/KL in He was also obtained by evacuating $H_2$ at 673 K and then filling with He before sealing with a flame.

## Results

**Hydrogen Chemisorption.** Hydrogen chemisorption isotherms for Pt/KL were obtained at 296 K. All the chemisorption isotherms were linear in the region of 5−50 kPa, similar to NaY zeolite entrapping a Pt cluster inside the supercage of 1.3 nm in diameter. Extrapolation of the linear part of the hydrogen chemisorption isotherm gave the *total* number of chemisorbed hydrogen atoms per Pt based on the *total* number of Pt atoms ($H_{total}/Pt_{total}$). As shown in Table 1, all the Pt/KL samples containing 0.9−5.2 wt % Pt chemisorbed the same number of hydrogen atoms per Pt within 1.9 ± 0.2 $H_{total}/Pt_{total}$. The

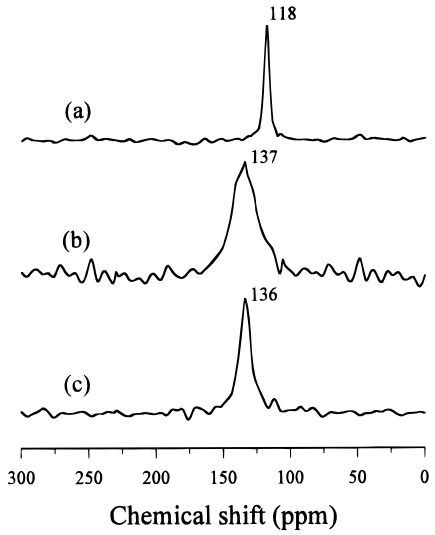


**Figure 1.** $^{129}$Xe NMR spectra for (a) KL zeolite, (b) 2.0 wt % Pt/KL, and (c) 2.0 wt % Pt/KL after $K^+$ ion exchange, obtained at 296 K and under 53.3 kPa.

**TABLE 1: Hydrogen Chemisorption and Catalytic Activity of *n*-Hexane Aromatization for Pt/KL**

| Pt (wt %) | $H_{total}/Pt_{total}$[a] | $\upsilon_t \times 100$ ($s^{-1}$)[b] | selectivity (%)[c] DHC[d]/ISO[e] |
|---|---|---|---|
| 0.9 | 1.9 | 13 | 62.8/37.2 |
| 2.0 | 1.7 | 10 | 45.8/54.2 |
| 3.4 | 2.0 | 8 | 48.0/52.0 |
| 5.2 | 2.0 | 5 | 48.3/51.7 |

[a] Total hydrogen chemisorption based on the total amount of Pt at 296 K. [b] Turnover frequency based on the total amount of Pt, with $H_2/C_6H_{14} = 6$ at 686 K. [c] At 15% conversion of *n*-hexane. [d] Dehydrocyclization products: benzene, methylcyclopentane, cyclohexene, and cyclohexane. [e] Isomerization and hydrogenolysis products: 2-methylpentane, 3-methylpentane, etc.

hydrogen chemisorption for Pt/KL is very high, compared with 1.2 $H_{total}/Pt_{total}$ obtained for Pt/NaY under the same experimental conditions.[10,11] Their difference in hydrogen chemisorption indicates that the Pt/KL cluster is smaller than the Pt/NaY cluster.

***n*-Hexane Aromatization.** Product distribution in *n*-hexane aromatization over Pt/KL is very similar to that reported in the literature,[3,9] giving benzene, methylcyclopentane, 2-methylpentane, 3-methylpentane, etc., at 686 K. The $\upsilon_t$ listed in Table 1 decreases from 0.013 to 0.005 as Pt loading increases from 0.9 to 5.2 wt %, showing decreases as much as 60%. A $\upsilon_t$ change to this decent extent is difficult to consider an intrinsic catalytic activity change owing to the cluster size variation among samples. On the contrary, the change in $\upsilon_t$ may be attributed to a diffusion limitation for the catalytic activity coming from a high concentration of Pt clusters located along the one-dimensional channel of the zeolite.

**$^{129}$Xe NMR Spectrum.** $^{129}$Xe NMR spectra of the Pt/KL samples obtained at 53.3 kPa at 296 K are shown in Figure 1. Each spectrum shows a single Lorentzian peak shifted downfield, compared with KL zeolite. The chemical shift comes from the Xe−Pt interaction inside the zeolite channels. Figure 2 shows that the chemical shift for the Pt/KL samples increases linearly with Pt content in the zeolite. The linear increase is very similar to the $^{129}$Xe NMR chemical shift changes with Pt content for Pt/NaY[7] and Pt/EMT,[11] which were attributed to increases in the number of Pt clusters without causing significant changes in the cluster size.

Reduction of Pt with $H_2$ subsequent to the ion exchange of $Pt(NH_3)_4^{2+}$ leads to the formation of two acidic $H^+$ ions per Pt in KL zeolite through the following reaction: $L_2\cdots Pt(II) + H_2 \rightarrow 2L\cdots H^+ + Pt(0)$, by the same reason as that for Pt/NaY,[13] where L denotes an ion exchange site of the zeolite. To exchange the acidic protons with $K^+$, the Pt/KL sample was exposed to air and then slurried in an aqueous solution of $KNO_3$. Subsequently, the sample was reduced at 573 K and evacuated at 673 K. The effect of the $K^+$ ion exchange for 2.0 wt % Pt/KL is shown in Figure 1b,c. The $K^+$ ion exchange treatment caused no changes in the hydrogen chemisorption and the $^{129}$Xe NMR chemical shift, indicating that the cluster size was not affected by the treatment for the $K^+$ ion exchange. However, the $^{129}$Xe NMR line width decreased markedly with the $K^+$ ion exchange. The effect on the $^{129}$Xe NMR line width may be attributed to the removal of solid state defects, similar to $Na^+$ ion exchange on HZSM-5 zeolite.[14] From the $K^+$ ion exchange effect, it seems that the Pt/KL may be exchanged with other cations without changing the Pt cluster size.

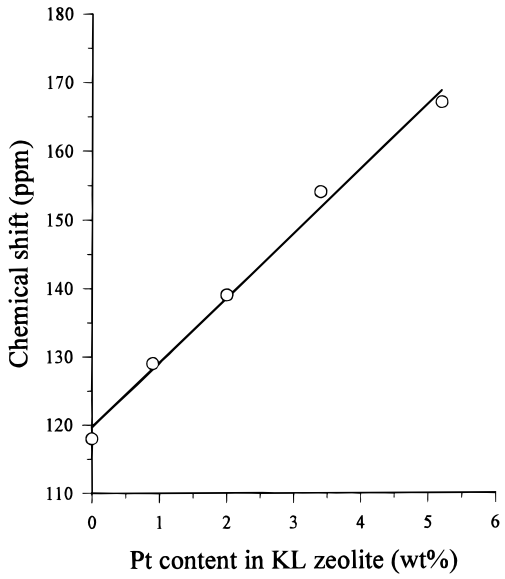


**Figure 2.** $^{129}$Xe NMR chemical shift of xenon adsorbed on Pt/KL samples at 296 K and under 53.3 kPa, plotted as a function of Pt content.

**Xenon Adsorption on the Pt Cluster.** Two xenon adsorption isotherms were obtained with each Pt/KL sample at 296 K, using a volumetric adsorption apparatus. The first xenon adsorption isotherm was obtained with *clean* Pt clusters after desorption of $H_2$ at 673 K. After the measurement of the first xenon adsorption isotherm, the sample was evacuated for longer than 30 min at 296 K. Subsequently, the sample was equilibrated with $H_2$ at 100 kPa and evacuated again at 296 K. This treatment gave the Pt clusters covered with irreversibly chemisorbed hydrogen, while the gas phase $H_2$ and the reversibly chemisorbed hydrogen were removed. The second xenon adsorption isotherm was obtained with the Pt cluster surface covered by the irreversibly chemisorbed hydrogen at 296 K. All the experiments were performed consecutively, keeping the same sample cell joined to the adsorption apparatus, and the sample temperature was precisely controlled using a constant-temperature circulator. Systematic errors during the adsorption measurements were canceled when the two adsorption isotherms were subtracted.

Figure 3 shows the two xenon adsorption isotherms thus obtained and their difference obtained for 2.0 wt % Pt/KL. Similar to xenon adsorption for Pt/NaY,[7,10] Pt/EMT,[11] Ru/NaY,[12] and Ir/NaY zeolites,[15] the amount of adsorbed xenon after the hydrogen chemisorption corresponds to the xenon adsorption occurring only on the zeolite support, while the amount without the hydrogen corresponds to the total xenon adsorption for the Pt/KL. The quantity of the second xenon adsorption decreased, compared with the first, because the chemisorbed hydrogen

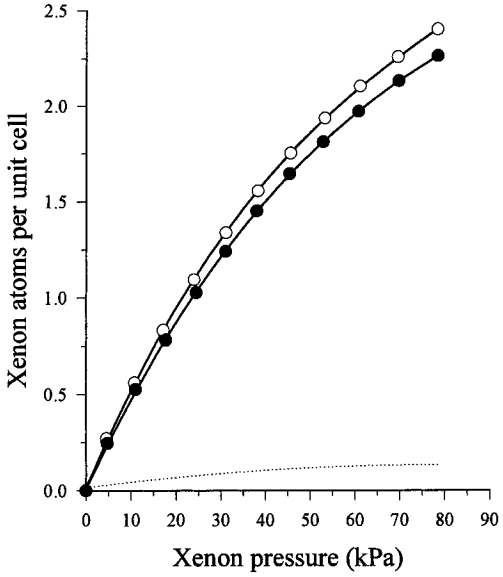


**Figure 3.** Xenon adsorption isotherms on a "fresh" 2.0 wt % Pt/KL sample (○) and after hydrogen chemisorption (●) at 296 K. The dotted line shows the difference between the two isotherms, which corresponds to a xenon adsorption isotherm for the Pt clusters supported on the KL zeolite.

inhibited xenon adsorption on the Pt cluster. The difference between the two xenon adsorption isotherms obtained respectively before and after the hydrogen chemisorption equals the amount of xenon adsorbed strongly on the *clean* Pt surface. The difference shown in Figure 3 may appear to be small. But, in fact, the difference was much larger than the error limits under the present experimental conditions. The amount of the xenon adsorption on the *clean* Pt surface thus obtained approached a saturation quantity corresponding to approximately 0.4 $Xe/Pt_{total}$ as pressure increased to 80 kPa. The saturation quantities for the xenon adsorption on the *clean* Pt surface for 3.4 wt % Pt/KL and 5.2 wt % Pt/KL were also approximately 0.4 $Xe/Pt_{total}$.

The xenon adsorption as much as 0.4 $Xe/Pt_{total}$ is very surprising, compared with 0.07 $Xe/Pt_{total}$ obtained for Pt/NaY in the same way. Assuming direct contact of Xe atoms on the surface of the Pt cluster at the saturation pressure, the 0.4 $Xe/Pt_{total}$ corresponds to the adsorption of two xenon atoms on a Pt cluster consisting of about four to six Pt atoms. Although the precision in the measurement is better than 5%, the accuracy of the obtained Pt cluster size depends very much on the assumption used in the estimation. It is also noteworthy that the pressure for the xenon adsorption saturation for Pt/KL is much higher than that (approximately 5 kPa) for Pt/NaY under the same experimental conditions.[7] The saturation of xenon adsorption on Pt/KL at high pressure indicates that the xenon adsorption on Pt/KL is weak compared with the Pt/NaY, probably due to a very small cluster size.

**X-ray Absorption Fine Structure.** XAFS for 2.0, 3.4, and 5.2 wt % Pt/KL samples were obtained above the Pt $L_{III}$ edge. The XAFS data in the wave vector ($k$) range between 30 and 140 $nm^{-1}$ were analyzed using the UWXAFS2 program package.[16] The extended X-ray absorption fine structure (EXAFS) oscillation ($\chi(k)$) was multiplied by the wave vector cube ($k^3$) after background removal and normalization. Background was removed with an $r$-space technique which minimized low-$r$ background components in the Fourier transform (FT) through the comparison with a standard XAFS generated using FEFF5 code.[17,18] The procedure is described in detail elsewhere.[19] Figure 4 shows the $k^3\chi(k)$'s obtained for Pt/KL

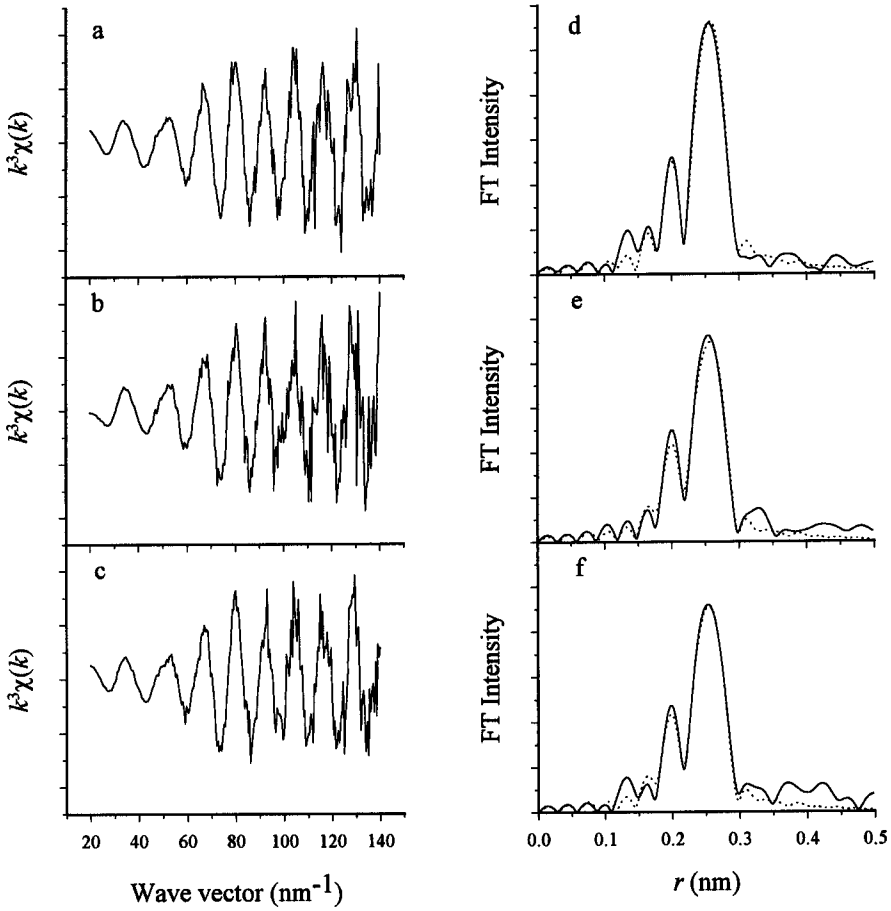


**Figure 4.** $k^3\chi(k)$-weighted EXAFS oscillation for Pt/KL samples and the Fourier transform in $r$-space: (a,d) 2.0 wt % Pt/KL; (b,e) 3.4 wt % Pt/KL; (c,f) 5.2 wt % Pt/KL. The best fitting EXAFS function is plotted as a dotted line in $r$-space.

**TABLE 2: Structural Parameters from EXAFS Curve Fit for Pt/KL**

| sample | pair | N[a] | $R$ (nm)[b] | $\sigma^2$ (pm$^2$)[c] | $\epsilon^2_\nu$[d] |
|---|---|---|---|---|---|
| 2.0 wt % Pt/KL[e] | Pt−Pt | 4.4 | 0.272 | 69 | 1.1 |
| 2.0 wt % Pt/KL[f] | Pt−Pt | 4.4 | 0.272 | 69 | 0.9 |
| | Pt−O | 0.2 | 0.279 | −20 | |
| 2.0 wt % Pt/KL[g] | Pt−Pt | 3.9 | 0.258 | 79 | 4.0 |
| 2.0 wt % Pt/KL[h] | Pt−Pt | 3.3 | 0.257 | 70 | 0.6 |
| | Pt−O | 3.5 | 0.256 | 584 | |
| 3.2 wt % Pt/KL[e] | Pt−Pt | 4.2 | 0.272 | 72 | 0.5 |
| 5.4 wt % Pt/KL[e] | Pt−Pt | 4.0 | 0.271 | 70 | 0.4 |

[a] Coordination number (±0.5). [b] Bond distance (±0.001 nm). [c] The Debye-Waller factor. [d] The reduced $\chi^2$ function defined in Ref. 23 [e] Samples in $H_2$, and curve fitting with Pt−Pt shell only. [f] Sample in $H_2$, and curve fitting with Pt−Pt and Pt−O shells. [g] Sample in helium, and curve fitting with Pt−Pt shell. [h] Sample in helium, and curve fitting with Pt−Pt and Pt−O shells.

samples in $H_2$ and the FT which were Fourier transformed from $30 \leq k \leq 140$ nm to $0.18 \leq r \leq 0.30$ nm using the Hanning window function.

The FT in Figure 4d,e,f show a peak at 0.2 nm (before the phase shift correction), where a peak due to the Pt−O coordination and a side-band coming from the Pt−Pt coordination can overlap each other. The side-band is known to appear for heavy-Z atoms with atomic numbers much greater than 40, due to complication or the oscillatory behavior in the backscattering amplitude function.[20] The sideband is so weak in intensity that it can be neglected for the EAXFS curve fitting in many cases, and the peak at 0.2 nm is due to the metal−oxygen bond. In the present study, however, the two kinds of contributions have been separated using an iterative curve-fitting technique with metal−metal and metal−oxygen standards. The curve fitting for the EXAFS was performed without Fourier filtering. The number of parameters used in the curve fitting was less than the allowed maximum number of parameters, $N_{\text{free}} = 2/\pi\ \delta r\ \delta k + 2$, where $\delta k$ is the FT range in $k$-space, and $\delta r$ is the fitting range in $r$-space.[21] The best curve fits thus obtained are shown as dotted curves in Figure 4. The structural parameters obtained through the curve fitting are listed in Table 2. The CN obtained from the EXAFS curve fitting were independent of Pt content of the zeolite within the curve-fitting error limits.

It is interesting to note that the nearest neighbor Pt−Pt distance for Pt/KL in helium was 0.256 nm, which contracted significantly from 0.277 nm for the bulk metal. The Pt−Pt and Pt−O CN were 3.3 and 3.5 in helium, respectively. The oxygen atoms were located at 0.257 nm from Pt. On the contrary, the Pt−Pt distance relaxed to 0.272 nm after hydrogen chemisorption. Furthermore, the Pt−Pt CN increased to 4.4 and the Pt−O coordination vanished after hydrogen chemisorption, which indicates reconstruction of the structure of the small Pt cluster in the KL zeolite channels.

**Xenon and $CCl_4$ Adsorption inside the Zeolite Channel.** Xenon adsorption isotherms of Pt/KL samples at 296 K are compared with a xenon adsorption isotherm of KL zeolite obtained under the same condition in Figure 5. The xenon adsorption decreased only slightly upon Pt loading as much as 5.2 wt %, which indicates that xenon was able to enter the one-dimensional zeolite channel in the presence of Pt clusters. If multiple pore blockage occurs due to Pt clusters in the channel, adsorption of xenon (diameter 0.43 nm) is expected to decrease much more. On the contrary, a small decrease in the xenon adsorption can occur due to substitution of $2K^+$ with $2H^+$ following the ion exchange of $Pt(NH_3)_4^{2+}$. A similar decrease in the xenon adsorption occurred when Pt was supported on NaY zeolite by ion exchange of $Pt(NH_3)_4^{2+}$.[7] This is also in agreement with increasing xenon adsorption upon exchanging $H^+$ with $K^+$ or $Na^+$ in zeolites.[22]

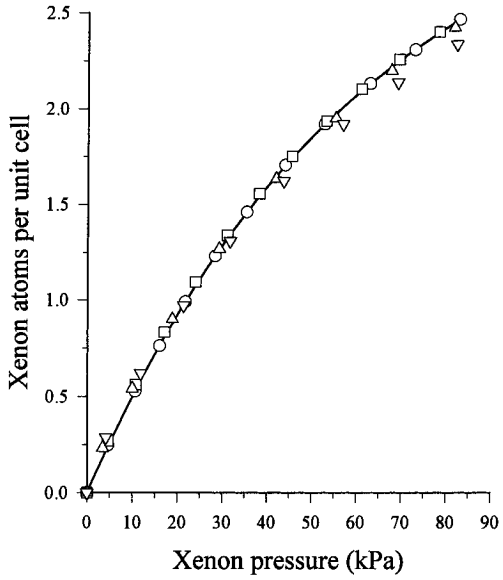


**Figure 5.** Xenon adsorption isotherms of KL zeolite (○), and fresh Pt/KL samples at 296 K: 2.0 wt % (□), 3.4 wt % (△), and 5.2 wt % (▽). The adsorption isotherms changed little while Pt content increased. The amount of xenon adsorption on Pt clusters (as shown in Figure 3) increased with the Pt content. But, the increase seemed to be compensated by a decrease in xenon adsorption in the zeolite wall, since xenon adsorption on $K^+$ decreased with increasing the $Pt(NH_3)_4^{2+}$ ion exchange.

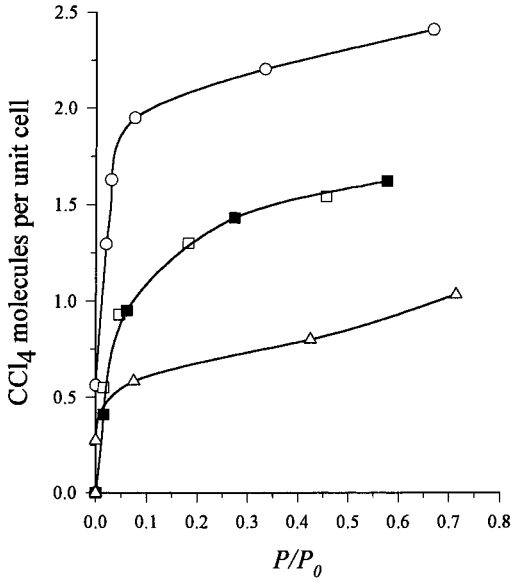


**Figure 6.** $CCl_4$ adsorption isotherms of KL zeolite (○), 2.0 wt % Pt/KL without chemisorbed hydrogen (□), 2.0 wt % Pt/KL with chemisorbed hydrogen (■), and 5.2 wt % Pt/KL without chemisorbed hydrogen (△) at 273 K.

As shown in Figure 6, adsorption of $CCl_4$ (diameter 0.59 nm) into the Pt/KL zeolite channel is severely limited due to the presence of Pt clusters. The $CCl_4$ adsorption quantity for the 2.0 wt % Pt/KL decreased by approximately 30%, compared with the KL zeolite. The adsorption quantity decreased further as Pt content increased to 5.2 wt %. Even if we assume that a Pt cluster consists of 13 Pt atoms, there will be a Pt cluster every 10 pores along the channel and the number of the Pt clusters present in a channel will be enough to block the adsorption much more than the decreases shown in Figure 6. From the $CCl_4$ adsorption quantities, it is considered that most Pt clusters were not large enough to cause the pore blockage for the $CCl_4$ adsorption. It is then reasonable to consider a cluster size distribution. The adsorption of $CCl_4$ into the KL

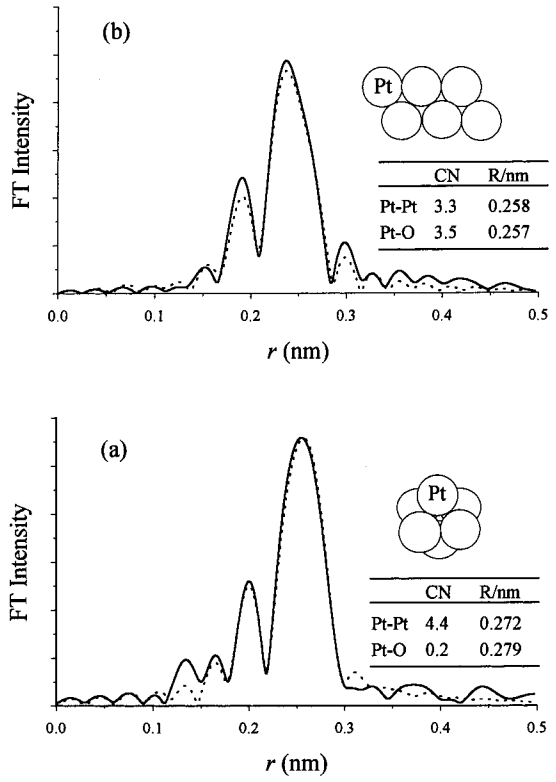


**Figure 7.** Fourier transforms of $k^3\chi(k)$-weighted EXAFS oscillation for 2.0 wt % Pt/KL in (a) dihydrogen and (b) helium. The best fitting EXAFS functions are plotted as a dotted line. Models of the clusters are also presented from the curve fit.

zeolite channel can be partly blocked by some clusters situated in the upper part of the cluster size distribution. Subtracting the size of $CCl_4$ (0.59 nm) from the diameter of the bulged part of the pore (1.1 nm), we can obtain 0.51 nm as the upper limit for the Pt cluster size which does not block the adsorption of $CCl_4$.

## Discussion

Figure 7a,b shows our best EAXFS curve fits obtained for 2.0 wt % Pt/KL in $H_2$ and helium atmospheres, respectively. The curve fits were obtained by taking into account both the Pt−Pt and Pt−O contributions given in Table 2. The curve-fitting error ($\epsilon^2_\nu$ defined in Table 2)[23] for the sample in helium increased significantly from 0.6 to 4.0 when the Pt−O contribution was neglected. On the contrary, the curve-fitting error for the sample in $H_2$ did not change significantly: $\epsilon^2_\nu \sim 0.9$ with the two-shell fitting and $\epsilon^2_\nu \sim 1.1$ with the one-shell. These different effects of the Pt−O shell on the curve-fitting errors give significance to the coordination numbers obtained within the error limit of ±0.5. The structural parameters in Table 2 indicate that the Pt cluster in $H_2$ was not coordinated to framework oxygen of the zeolite. For the cluster without the Pt−O coordination, we may assume that Pt atoms were closely packed to give maximum contact with each other. A model of such a closely packed cluster that can give the Pt−Pt CN as close to 4.4 as possible is shown in Figure 7a. The diameter of the Pt cluster is approximately 0.5 nm, which is close to the upper limit (0.51 nm) imposed by the $CCl_4$ adsorption. Compared with the $H_2$ atmosphere, the bare Pt cluster in the helium gave a large Pt−O CN (3.5) and a small Pt−Pt CN (3.3). These changes in the coordination numbers indicate that the bare Pt cluster was closely attached to oxygen atoms of the zeolite framework. A model for a Pt cluster consistent with the CN is presented in Figure 7b. Thus, the results from EXAFS curve fitting suggest a morphological transformation due to the hydrogen chemisorption−desorption.

It was reported that Pt atoms in very small clusters in helium or under vacuum spread onto the zeolite surface,[24] thus maximizing the metal−support interaction or minimizing the surface stress.[25] Koningsberger and Gates[26] reported the Pt−O coordination in the range 0.25−0.27 nm as evidence of the characteristic interaction between zero-valent Pt atom and support oxygen. Our Pt−O CN of 3.5 with the distance at 0.256 nm agrees with the metal−support interaction under helium atmosphere. It is indicated that each Pt atom in the Pt cluster in helium was coordinated with three or four oxygen atoms on the average, with the very large Debye−Waller factor, 584 $pm^2$. However, when the Pt cluster chemisorbed hydrogen in $H_2$ atmosphere, the chemisorbed hydrogen seemed to inhibit the Pt−O interaction and therefore allowed a morphological change to achieve a highest possible Pt−Pt CN.

Another interesting point observed with the hydrogen chemisorption on Pt/KL is relaxation in the Pt−Pt distance. Similar effects of the hydrogen chemisorption for the metal−metal bond distance were reported for group VIII metal clusters supported on NaY zeolites.[27] The effects of hydrogen chemisorption on small metal clusters are very similar to the adsorbate induced surface reconstruction for the Pt(100) plane.[28] The surface reconstruction by adsorbate-atoms was also reported for H on Ni(110)-1×2[29] and Pd(110).[30] Generally, the bond contraction is known to increase as the metal−metal CN for the surface atom decreases. The reconstruction of the surface atomic structure is believed to be due to the metal−metal and metal−adsorbate pairwise attraction.[31] Therefore, the contraction in the Pt−Pt bond distance for Pt/KL is not only due to the metal−support interaction but also somewhat intrinsic of the surface nature.

The models of the Pt cluster derived from our XAFS curve fitting agree with the number of Pt atoms per cluster obtained using our xenon adsorption method. The cluster size did not change while the Pt content in the KL zeolite was increased from 0.9 to 5.2 wt %. Moreover, the hydrogen chemisorption, $1.9 \pm 0.2$ $H_{total}/Pt_{total}$, which was independent of the Pt content, indicates the absence of the effect of hydrogen spillover. Clearly, each Pt atom chemisorbed two hydrogen atoms. We believe that the hydrogen chemisorption lower than 2.0 H/Pt in other works on Pt/KL can be due to agglomeration of Pt atoms into clusters larger than the cluster size which we obtained here. It is therefore important to increase the temperatures for the sample activation and reduction very slowly, to prevent the cluster size growth. We attempted to measure the Pt cluster size using transmission electron microscopy (TEM) but failed to detect them due to very small size, below the resolution of our TEM, while 1-nm Pt clusters in the supercages of zeolites NaY and EMT were detected easily under the same conditions.[10,11]

According to our $^{129}Xe$ NMR chemical shift measurement, the Pt cluster supported on KL zeolite was located inside the one-dimensional zeolite channel. Assuming that each cluster consisted of six Pt atoms and the zeolite channel was 1 $\mu$m long, the number of the clusters along a channel of 0.9, 2.0, 3.4, and 5.2 wt % Pt/KL samples can roughly be estimated as 40, 80, 140, and 210, respectively. If pore blockage occurred due to the presence of so many Pt clusters along the one-dimensional zeolite channel, the channel inside should be inaccessible for the adsorption of Xe (0.43 nm in kinetic diameter), *n*-hexane (0.60 nm), benzene (0.69 nm), and $CCl_4$ (0.59 nm), and consequently both xenon adsorption and the catalytic conversion of *n*-hexane should occur very little. However, our results from adsorption and catalytic reaction

measurements are contrary to the multiple pore blockage.[5,9,32,33] The Pt cluster size obtained in the present work is very small, compared with previous results obtained by Haller and co-workers.[5,33] Our result agrees with the conclusion of five to six atoms per cluster drawn by Vaarkamp et al. using the Pt−Pt CN.[4,24]

It is remarkable that the Pt cluster inside the KL zeolite cage consisted of only six Pt atoms, in contrast to previous results from xenon adsorption for Pt/NaY indicating agglomeration of 50−60 Pt atoms inside the supercage.[7,10] The same method was used for the preparation of Pt clusters in both zeolites. The xenon adsorption method and XAFS curve fitting were used exactly in the same ways. In both cases, the cluster size was independent of Pt content. However, the number of Pt atoms per cluster in KL zeolite was much smaller than that in NaY. Previously, we attributed the formation of the cluster in the supercage to the metal−support interaction that could be maximized by filling the entire volume of the supercage with Pt atoms.[7] There is no large difference between the sizes of the two zeolite apertures. Both zeolite apertures consist of a 12-membered oxygen ring with 0.7−0.8 nm in diameter. The cage diameters are not very different: 1.3 nm for NaY and 1.1 nm for KL. The cage aperture of the KL zeolite is not small enough to confine the six-atom Pt cluster. The cluster size could increase during heating to 673 K by migration through the cage aperture if the cluster had high mobility. Considering all these points, we believe that the metal−support interaction is strong enough to hold the six-atom cluster inside the KL zeolite cage. The strong interaction site may be $K^+$ ions or the elliptically distorted eight-membered oxygen ring on the wall of the KL zeolite cage.

Sachtler and co-workers[34] have suggested that small Pt clusters supported on zeolite Y can be partially oxidized by zeolite protons upon desorption of dihydrogen due to a shift in the following equilibrium: $Pt^0 + 2L\cdots H^+ \rightarrow 2L\cdots Pt^{2+} + H_2\uparrow$. It is expected that changes in the oxidation state for the Pt cluster can be reflected in the X-ray absorption near edge structure (XANES), following the XANES analysis method reported by Moraweck et al.[35] Moraweck et al. showed that the Pt XANES changed at both the Pt $L_{III}$ and $L_{II}$ edges upon alloying Pt with Ni. The allowed transitions corresponding to the Pt $L_{III}$ XANES are $2p_{3/2} \rightarrow 5d_{3/2}$ and $5d_{5/2}$, while the transition for the Pt $L_{II}$ XANES is $2p_{1/2} \rightarrow 5d_{3/2}$. Therefore, quantitative information on electron vacancy in the $5d_{3/2}$ band can be obtained from $A_{III} - kA_{II}$, where $A$ is the area under the XANES peak, and $k$ is a constant considering the transition probability. In the work of Moraweck et al., there was a distinct change in the electron vacancy, indicating electron transfer between the metals. We have analyzed Pt XANES for Pt/KL in the same way. However, the present work indicates no detectable change in the electronic structure for Pt/KL under helium atmosphere, compared with that of Pt foil, as Figure 8 shows. Thus, the XANES shows no changes in the electronic structure that are indicative of the Pt oxidation state by zeolite protons. Moreover, the analysis of the Pt XANES shows no difference between the small supported Pt cluster and bulk Pt foil. The result may be similar because the information obtained from the XANES analysis technique can be limited to only the $5d_{5/2}$ state of the Pt atom.

## Conclusion

It can be concluded that the Pt cluster in our KL zeolite consists of approximately six Pt atoms. The cluster is clearly located inside the one-dimensional channel of the zeolite. The Pt cluster in helium atmosphere seems to be somewhat flattened and strongly attached to the zeolite wall, due to the metal−support interaction. Upon hydrogen chemisorption, the Pt cluster loses the metal−support interaction and therefore undergoes a morphological change to a more spherically close packed one. The nearest neighbor Pt−Pt distance in the Pt cluster in helium is 0.257 nm, showing a lattice contraction, compared with 0.277 nm for bulk Pt metal. The Pt−Pt distance relaxes to 0.272 nm when the cluster chemisorbs hydrogen.

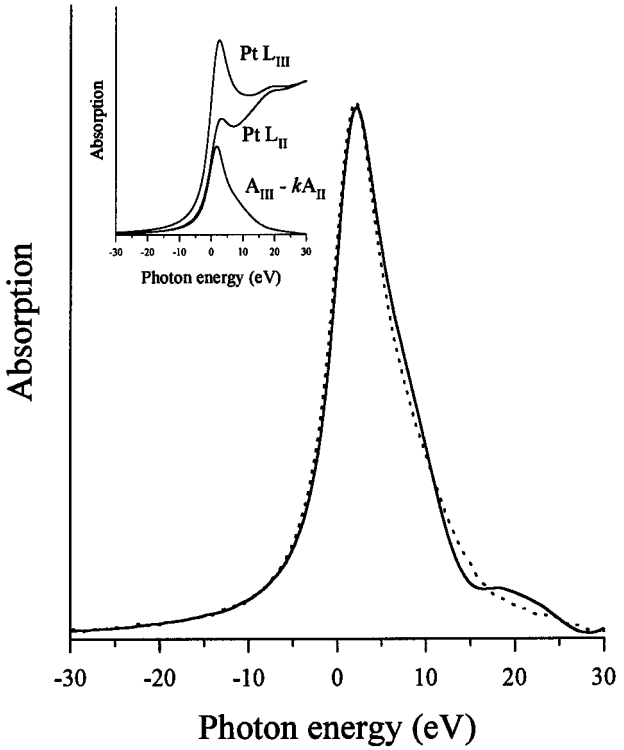


**Figure 8.** Difference spectra of XANES for 2.0 wt % Pt/KL under helium (···) and Pt foil (—). The photon energy was corrected for $E_0$, which was the first zero of the second derivative in the X-ray absorption. XANES spectra above the $L_{III}$ edge and $L_{II}$ edges of the 2.0 wt % Pt/KL sample in helium are shown in the inset, with their difference.

The Pt cluster in the KL zeolite channel is so small that it does not cause pore blockage for the adsorption of xenon atoms and $CCl_4$ molecules severely. Under these circumstances, it is reasonable that the catalytic conversion of *n*-hexane to benzene occurs over the Pt cluster inside the zeolite channel.

**Acknowledgment.** The authors thank the Photon Factory (Proposal No. 95G197) and Pohang Accelerator Laboratory for their support for the XAFS measurements.

## References and Notes

(1) Breck, D. W. *Zeolite Molecular Sieves-Structure, Chemistry, and Use*; Wiley; New York, 1974, p 636.

(2) Tauster, S. J.; Steger, J. J. *J. Catal.* **1990**, *125*, 387.

(3) (a) Bernard, J. R. In *Proc. 5th Int. Conf. Zeolites*; Rees, L. V. C., Ed.; Heyden: London; 1980; p 686. (b) Davis, R. J.; Derouane, E. G. *Nature* **1991**, *349*, 313. (c) Hong, S. B.; Mielczarski, E.; Davis, M. E. *J. Catal.* **1993**, *134*, 349. (d) Gates, B. C. *Chem. Rev.* **1995**, *95*, 511.

(4) Vaarkamp, M.; Grondelle, J. V.; Miller, J. T.; Sajkowski, D. J.; Modica, F. S.; Lane, G. S.; Gates, B. C.; Koningsberger, D. C. *Catal. Lett.* **1990**, *6*, 369.

(5) McHugh, B. J.; Larsen, G.; Haller, G. L. *J. Phys. Chem.* **1990,** *94*, 8621.

(6) Derouane, E. G.; Vendervekeen, D. *J. Appl. Catal.* **1988**, *45*, L15.

(7) (a) Ryoo, R.; Cho, S. J.; Pak, C.; Kim, J.-G.; Ihm, S.-K.; Lee, J. Y. *J. Am. Chem. Soc.* **1992**, *114*, 76. (b) Hughes, J. R.; Buss, W. C.; Tamm, P. W.; Jacobson, R. L. In *Studies in Surface Science and Catalysis*; Murakami, Y., et al., Eds.; *New Developments in Zeolite Science and Technology*; Elsevier Science: Amsterdam, 1986; Vol. 28, p 725.

(8) Unpublished results.

(9) Sharma, S. B.; Ouraipryvan, P.; Nair, H. A.; Balarman, P.; Root, T. W.; Dumesic, J. A. *J. Catal.* **1994**, *150*, 234.

(10) Ryoo, R.; Cho, S. J.; Pak, C.; Lee, J. Y. *Catal. Lett.* **1993**, *20*, 107.

(11) Ihee, H.; Becue, T.; Ryoo, R.; Potvin, C.; Manoli, J.-M.; Djega-Mariadassou, G. In *Studies in Surface Science and Catalysis*; Weitkamp, J., et al., Eds.; *Zeolites and Related Microporous Materials: State of the Art 1994*; Elsevier Science: Amsterdam, 1994; Vol. 84, p 765.

(12) Cho, S. J.; Jung, S. M.; Shul, Y. G.; Ryoo, R. *J. Phys. Chem.* **1992,** *96*, 9922.

(13) (a) Chow, M.; Park, S. H.; Sachtler, W. M. H. *Appl. Catal.* **1985**, *19*, 349. (b) Bai, X.; Sachtler, W. M. H. *J. Catal.* **1991**, *129*, 121.

(14) Ryoo, R.; Ihee, H.; Kwak, J. H.; Seo, G.; Liu, S.-B. *Microporous Materials* **1995**, *4*, 59.

(15) Pak, C.; Cho, S. J.; Lee, J. Y.; Ryoo, R. *J. Catal*. **1994**, *149*, 61.

(16) Frenkel, A. I.; Stern, E. A.; Qian, M.; Newville, M. *Phys. Rev. B* **1993**, *48*, 12449.

(17) Newville, M.; Livins, P.; Yacoby, Y.; Rehr, J. J.; Stern, E. A. *Phys. Rev. B* **1993**, *47*, 14126.

(18) Rehr, J. J.; Albers, R. C.; Zabinsky, S. I. *Phys. Rev. Lett*. **1992,** *69*, 3397.

(19) Frenkel, A.; Stern, E. A.; Voronel, A.; Qian, M.; Newville, M. *Phys. Rev. B* **1994**, *49*, 11662.

(20) Rabe, P.; Tolkiehn, G.; Werner, A. *J. Phys. C: Solid State Phys.* **1979**, *12*, 899.

(21) Stern, E. A. *Phys. Rev. B* **1993**, *48*, 9825.

(22) Kim, J. G.; Ihm, S.-K.; Lee, J. Y.; Ryoo, R. *J. Phys. Chem*. **1991**, *95*, 8546.

(23) (a) Binsted, N.; Strange, R. W.; Hasnain, S. S. *Biochemistry* **1992**, *31*, 12117. (b) The UWXAFS2 manual, University of Washington, 1993.

(24) Vaarkamp, M.; Miller, J. T.; Modica, F. S.; Lane, G. S.; Koningsberger, D. C. *J. Catal*. **1992,** *138*, 675.

(25) Balerna, A.; Bernieri, E.; Picozzi, P.; Reale, A.; Santucci, S.; Burattini, E.; Mobilio, S. *Phys. Rev. B* **1985**, *31*, 5058.

(26) Koningsberger, D. C.; Gates, B. C. *Catal. Lett.* **1992**, *14*, 271.

(27) (a) Cho, S. J.; Pak, C.; Ryoo, R. In preparation. (b) Moraweck, B.; Clugnet, G.; Renouprez, A. J. *Surf. Sci.* **1979**, *81*, L631.

(28) Inglesfield, E. J. *Progr. Surf. Sci*. **1985,** *20*, 105.

(29) Christmann, K.; Penka, V.; Chehab, F.; Ertl, G.; Behm, R. J. *Solid State Commun*. **1984**, *51*, 487.

(30) Cattania, M. G.; Penka, V.; Behm, R. J.; Christmann, K.; Ertl, G. *Surf. Sci*. **1983**, *126*, 382.

(31) Somorjai, G. A. *Chemistry in Two Dimensions: Surfaces*; Cornell University Press; Ithaca, 1981.

(32) McVicker, G. B.; Kao, J. L.; Ziemiak, J. J.; Gates, W. E.; Robbins, J. L.; Treacy, M. M. J.; Rice, S. B.; Venderspurt, T. H.; Cross, V. R.; Ghosh, A. K. *J. Catal*. **1993**, *139*, 48.

(33) Larsen, G.; Daniel, E. R.; Durante, V. A.; Kim, J.; Haller, G. L. In *Studies in Surface Science and Catalysis*; Hattori, M., Yashima, T. Eds.; *Zeolites and Microporous Crystals*; Kodansha: Tokyo, 1994; Vol. 83, p 321.

(34) Tzou, M. S.; Jiang, H. J.; Sachtler, W. M. H. *React. Kinet. Catal. Lett.* **1987**, *35*, 207.

(35) Moraweck, B.; Renouprez, A. J.; Hlil, E. K.; Baudoing-Savois, R. *J. Phys. Chem.* **1993**, *97*, 4288.

JP952594B